Translational regulation via L11: Molecular switches on the ribosome turned on and off by thiostrepton and micrococcin

Joerg M. Harms[1,2,*], Daniel N. Wilson[2,3,4,8,*], Frank Schluenzen[2,5,*], Sean R. Connell[1,6], Torsten Stachelhaus[7,#], Zaneta Zaborowska[1], Christian M. T. Spahn[6] and Paola Fucini[1,2,8]

[1] Cluster of Excellence for Macromolecular Complexes, Institute fuer Organische Chemie und Chemische Biologie, J. W. Goethe-Universitaet Frankfurt am Main, Max-von-Laue-Strasse 7, D-60438 Frankfurt am Main, Germany

[2] Max-Planck-Institute for Molecular Genetics, AG-Ribosomen, Ihnestr. 73, D-14195 Berlin, Germany

[3] Gene Center and Department of Chemistry and Biochemistry, University of Munich, LMU, Feodor Lynen Str. 25, 81377, Munich, Germany

[4] Munich Centre for Integrated Protein Science, University of Munich, Germany

[5] Deutsches Elektronen-Synchrotron (DESY), Notkestr. 85, D-22603 Hamburg, Germany

[6] Institut für Medizinische Physik und Biophysik, Charite - Universitätsmedizin Berlin, Ziegelstrasse 5-9, 10117 Berlin, Germany

[7] Department of Chemistry/Biochemistry, Philipps University of Marburg, Hans-Meerwein-Str., D-35032 Marburg, Germany

[8] Correspondence: fucini@chemie.uni-frankfurt.de, wilson@lmb.uni-muenchen.de

* These authors contributed equally to this work

present address: AureoGen Biosciences, Inc., 6475 Technology Ave. (Suite C), Kalamazoo, MI 49009, USA

Summary

The thiopeptide class of antibiotics targets the GTPase-associated center of the ribosome to inhibit translation factor function. Using X-ray crystallography, we have determined the binding sites of thiostrepton, nosiheptide and micrococcin, on the *Deinococcus radiodurans* large ribosomal subunit. The thiopeptides, by binding within a cleft located between the ribosomal protein L11 and helices 43 and 44 of the 23S rRNA, overlap with the position of domain V of EF-G, thus explaining how this class of drugs perturb translation factor binding to the ribosome. The presence of micrococcin leads to additional density for the C-terminal domain (CTD) of L7, adjacent to and interacting with L11. The results suggest that L11 acts as a molecular switch to control L7 binding and plays a pivotal role in positioning one L7-CTD monomer on the G' domain of EF-G to regulate EF-G turnover during protein synthesis.

Running title: Thiopeptide-mediated translation factor inhibition on the ribosome

Keywords: antibiotics / elongation factor G / EF-G / GTPase / protein synthesis / ribosome / micrococcin / nosiheptide / thiostrepton / translation / L7 / L11

Introduction

The protein synthesizing apparatus, the ribosome, is one of the major targets in the cell for natural antibiotics (reviewed by Spahn and Prescott, 1996; Wilson, 2004). In the past seven years, significant progress has been made in the determination of structures of ribosomal subunits in complex with many of the major classes of antibiotics (reviewed by Wilson, 2004). These structures have provided insight into the mechanism of action of antibiotics, revealing that they bind almost exclusively to ribosomal RNA (rRNA) and target the active sites of the prokaryotic ribosome, such as the decoding site on the 30S subunit and the peptidyltransferase centre on the 50S subunit. However, another important region for ribosome function is the "factor binding site", which encompasses the so-called GTPase-associated center (GAC), responsible for binding and stimulation of the GTPase activity of translation factors from all phases of translation. Unlike other active sites, the GAC is rich in ribosomal proteins (r-proteins) as well as rRNA. Three GAC components considered to be important for GTPase activation of translation factors include (i) the sarcin-ricin loop (SRL) located in helix 95 (H95) of the 23S rRNA, (ii) the ribosomal stalk, composed of r-proteins L10 and 4-6 copies of L7/L12, and (iii) the stalk base (SB), comprising L11 and its binding site on the 23S rRNA, namely H43 and H44 (reviewed by Wilson and Nierhaus, 2005).

The thiopeptide family includes some of the best studied antibiotics in the field of translation, such as thiostrepton (Thio) and micrococcin (Micro), as well as the lesser known nosiheptide (Nosi) (reviewed by Spahn and Prescott, 1996; Wilson, 2004). These antibiotics bind the SB and, unlike most other antibiotics, target both r-protein (L11) as well as (23S) rRNA. The cooperative nature of the binding is highlighted by the fact that Thio cannot bind free L11 (Highland and Howard, 1975; Porse et al., 1998), and, although it can bind naked 23S rRNA, the affinity is much lower (~10^3) than that for the intact ribosome (Bausch et al., 2005; Thompson et al., 1979). Moreover, resistance to Thio and Micro can be obtained by

deletion or mutations in the *rplK* gene encoding L11 (Cameron et al., 2004; Cundliffe et al., 1979; Porse et al., 1999; Porse et al., 1998; Wienen et al., 1979), as well as transversions and transitions of A1067 or A1095 (*Escherichia coli* numbering is used throughout) in H43 or H44, respectively, of the 23S rRNA (Cameron et al., 2004; Hummel and Boeck, 1987; Mankin et al., 1994; Rosendahl and Douthwaite, 1993).

Of the thiopeptides, the effect of Thio and Micro on the action of EF-G has been most intensively studied (Bowen et al., 2005; Cameron et al., 2002; Lentzen et al., 2003; Rodnina et al., 1999; Seo et al., 2006; Seo et al., 2004). Traditionally, Micro has been documented as a stimulator of the GTPase activities of EF-G (Cameron et al., 2002) while Thio is considered a factor-specific translocation inhibitor that prevents the EF-G catalyzed movement of the A- and P-tRNAs (PRE state) to the P- and E-sites (POST state) of the ribosome (Cameron et al., 2002; Lentzen et al., 2003). The differential effect of Thio and Micro on EF-G GTPase is intriguing, since the two drugs have similar structures and are expected to bind in the same region of the ribosome.

The low solubility of thiopeptides led to the difficulty in the use of these compounds within the clinical setting, however there has been renewed interest due to (i) the discovery of fragments of Thio that have biological activity (Nicolaou et al., 2005a), (ii) a complete description for the total synthesis of Thio now being available (Nicolaou et al., 2005b), and (iii) the finding that both Thio and Micro inhibit not only bacteria, but also the growth of the human malarial parasite *Plasmodium falciparum* by acting on the ribosomes of the plastid-like organelle (Rogers et al., 1998). However, development of more potent thiopeptide inhibitors requires a better structural understanding of how these compounds interact with ribosome to exert their differential effects of factor-dependent GTPase activities.

In this study we have determined the binding sites of the thiopeptides, Thio, Nosi and Micro, on the *Deinococcus radiodurans* large ribosomal subunit. All three thiopeptides bind within a cleft located between the L11-NTD and the loops of H43 and H44 of the 23S rRNA,

in good agreement with the wealth of available biochemical data related to these compounds. Unexpectedly, the binding of Micro leads to the appearance of density for one CTD of r-protein L7/L12 (L7-CTD). The L7-CTD contacts L11 and is located in the same relative position as additional density assigned to L7-CTD in our recent cryo-electron microscopy (cryo-EM) reconstruction of EF-G bound to a 70S ribosome (Connell et al., 2007). Coupled with the stimulatory effect that Micro, but not Thio or Nosi, have on EF-G-dependent GTPase, leads us to present a model whereby two molecular switches are present in L11 that play a pivotal role during translation elongation to position one of the L7-CTD to interact with the G' domain of EF-G, and thus promote rapid and efficient EF-G turnover during protein synthesis.

Results

The binding position of the thiopeptide antibiotics on the ribosome

Datasets from crystals of the *D. radiodurans* large ribosomal subunit (D50S) in complex with the thiopeptide antibiotics, Thio, Nosi and Micro, were collected at a resolution of 3.3-3.7 Å (**Supplemental Table 1**). Thio comprises 16 chemical moieties that can be grouped into two loops and a tail (**Figure 1A**). While the first loop is conserved in both Nosi and Micro, loop2 is shorter (and connected differently) in Nosi, and totally absent in Micro (**Figure 1A-C**). In each reconstruction obtained, the electron density for the L11-NTD was significantly improved compared to the native D50S and additional ring-like density, which was attributed to the drug, was observed in a cleft between the L11-NTD and the tips of H43 and H44 of the 23S rRNA, (**Figure 2A**). The availability of small molecule structures of Thio (Bond et al., 2001) and Nosi (Prange et al., 1977) enables an accurate fitting of the drug structure to the density for these two compounds (**Figure 2B** and **C**).

The density for Micro indicates that the drug does not bind in the same position as Thio or Nosi, with loop1 being displaced by ~6 Å when compared to Thio (**Figure 5B**). The resolution limitations and absence of a 3D small molecule structure for Micro prohibited precise determination of the molecular interactions. Nevertheless we generated a model for Micro based on the similarities between Micro and Nosi (**Figure 1B** and **1C**), which serves as a placeholder for the position of the drug, and allows the differential activities of Micro with respect to Thio to be elucidated.

Interaction of thiostrepton and nosiheptide with the ribosome

The interaction of Thio and Nosi with the ribosome is predominantly hydrophobic, analogous to the binding of the lactone rings of the macrolide class of antibiotics (Hansen et al., 2002). Consistent with the conservation of loop1 in the Thio and Nosi structures (**Figure 1A** and **1B**), this loop inserts into the cleft between L11-NTD and the 23S rRNA, and constitutes the predominant interactions between the drug and the ribosome. Loop2 moieties, with the exception of the quinaldic acid (QA) group, which approaches H44, are solvent exposed. Accordingly, of the 620 $Å^2$ of surface that Thio buries on the ribosome, 60% are attributable to loop1 residues, whereas the tail and loop2 contribute 26% and 14%, respectively.

The sulfur-containing thiazole rings in loop1 and the tail, which give this class of antibiotic their name, are positioned to stack on either the bases of RNA nucleosides or the aromatic side-chains of amino acids in the L11-NTD. (However, it should be noted that the geometry is not optimal for Pi-stacking interactions, so stacking is used in a more generic sense here.) In particular, THZ6 and THZ14 of Thio (refer to **Figure 1** for the different moieties of the drug) stack on Pro22 and Pro26 of L11, respectively, while THZ1 is oriented to form stacking interactions with A1095 of the 23S rRNA (**Figure 3A** and **3B**). It has been suggested that the QA moiety of Thio is engaged in Pi-stacking interaction with the base of

A1067 (Lentzen et al., 2003), however, although the QA moiety approaches the A1067 in the structure, the orientation, geometry and distance preclude any significant stacking interaction. The QA moiety of Thio does, however, come within 3.5 Å of the N1 of A1067, explaining why Thio protects this position from chemical attack by dimethylsulfate (DMS) (Bowen et al., 2005; Egebjerg et al., 1989; Rosendahl and Douthwaite, 1993). The THZ1 ring of Thio stacks onto the base of A1095 and comes within 3.5 Å of the N7, whereas the neighboring residues (THR2 and DHB3) in loop1 approach within 4-5 Å of the N1 of A1095, consistent with protection by Thio of these positions from chemical probing using diethylpyrocarbonate and DMS, respectively (Egebjerg et al., 1989).

Superimposing the small molecule structure of Thio, on the basis of loop1, positions the tail of the drug extending out into the solvent such that no contacts with the ribosome are possible (**Figure 3C**). However, in the bound state, the tail of Thio is reoriented compared to the small molecule structure, reaching over alpha-helix 1 (α1) in the L11-NTD and contributing significantly to the overall interaction area (26%). This placement of the tail seems to induce a conformational change in L11 so that the position of both α1 as well as the distal end (N-terminal β-strand (β1) and loop between β2 and β3) of L11-NTD are shifted relative to their position in the native D50S structure (**Figure 3D**). Interestingly, a similar conformational switch in the L11-NTD is observed when Nosi binds to the D50S (**Figure 3E**). In this case, however, the tail of Nosi runs parallel to α1 passing under Gln30, rather than reaching over it as Thio does. Nevertheless, Nosi apparently induces a similar shift in L11-NTD by encroaching on the position that α1 normally occupies in the native D50S structure. Consistent with the conformational switch observed in this region, the presence of Thio has been shown to protect Tyr62, located in the loop between β2 and β3, and to a lesser extent Phe38 (α2) and Phe67 (β3) from chymotrypsin cleavage (Porse et al., 1998).

As well as being consistent with the biochemical data, the binding position of Thio determined here crystallographically is in good agreement with a model for the loop1 and 2

moieties of Thio produced by Lentzen and colleagues from NMR restraints (Lentzen et al., 2003). However the exact placement of Thio differs slightly from the NMR model: When aligning the two structures on the basis of H43 and H44 (r.m.s.d. = 1.3 Å) the position of Thio is shifted (3-4 Å), leading to slight changes in the interaction with the ribosome, such as the aforementioned stacking between the QA moiety of Thio and the base of A1067. The interaction between Thio and the rRNA as seen in the more recent NMR-derived model (Jonker et al., 2007) exhibits also some differences (**Supplemental Figure 1**) with respect to the structure presented here, which may result from the fact that a mutant rRNA fragment was used for H43/44.

Thiopeptide resistance in prokaryotes and eukaryotes

Mutations at position A1067 in H43 or A1095 in H44 confer resistance to thiostrepton in *E. coli* (Rosendahl and Douthwaite, 1994; Thompson et al., 1988). Both adenines are conserved in all prokaryotic 23S rRNA sequences (**Supplemental Figure 2**) and mutations of the equivalent positions in *Thermus thermophilus* (Cameron et al., 2004), and A1067U/G mutations in the archaea *Halobacterium halobium* and *H. cutirubrum* (Hummel and Boeck, 1987), also confer Thio resistance. The tertiary structure of H43 and H44 in the D50S is essentially identical to that observed in *E. coli* (Schuwirth et al., 2005) and *Haloarcula marismortui* (Ban et al., 2000) ribosome structures, as well as the L11-RNA complex from *Thermotoga maritima* (Wimberly et al., 1999). Therefore it is likely that Thio binds in a similar fashion to all prokaryotic ribosomes and that the mechanism of resistance is analogous.

The Thio-D50S structure presented here reveals that A1067 and A1095 in H43 and H44 make the most extensive contact with the drug, with the only other significant interaction involving the ribose of G1068. A1067 and A1095 are located at the tips of their respective helices and form a platform upon which Thio sits (**Figure 2A** and **3A**). Footprinting

experiments demonstrate that mutation of A1067 or A1095 to a pyrimidine (U or C) reduces Thio binding (1000-fold as measured by monitoring the protection of A1095) more effectively than the A1067G purine transversion (Rosendahl and Douthwaite, 1994). Furthermore, a 3-fold excess (40nM) of Thio over ribosomes can inhibit EF-G-dependent GTP hydrolysis on wildtype (60%) and A1067G (21%), but not on A1067U ribosomes (Cameron et al., 2004). Indeed for the A1067 mutations, a correlation between the loss in Thio binding and the level of Thio resistance has been previously observed (Thompson et al., 1988). In the Thio-D50S structure, a pyrimidine at either A1067 or A1095 would provide less surface area for stacking or hydrophobic interactions than a purine, providing a possible explanation for how such mutations would reduce the affinity of Thio to confer higher levels of resistance. However, conformational changes within the loop structures induced by these mutations that prevent or reduce drug binding cannot be ruled out. The producer of Thio, *Streptomyces azureus*, inhibits drug binding to its own rRNA by 2'-O-methylation of position A1067 (Thompson et al., 1982). The 2'O of A1067 is within 3.1 Å of the THZ4 (**Figure 3B**) and therefore the presence of an additional methyl group would prevent the close approach of loop1 of Thio to H43, analogous to mechanism by which (di-)methylation of the N6 of A2058 confers resistance to macrolides such as erythromycin (Hansen et al., 2002).

The L11-NTD constitutes ~50% (314 $Å^2$) of the buried surface area (620 $Å^2$) of Thio, explaining why the absence of L11 dramatically reduces the affinity of Thio (and Micro) for the ribosome to confer resistance (Cundliffe et al., 1979; Thompson et al., 1979) as well as explaining the cooperative nature of rRNA and L11-NTD for Thio binding (Xing and Draper, 1996). It is also possible to rationalize how point mutations within the L11-NTD confer varying degrees of Thio resistance (Cameron et al., 2004; Porse et al., 1999; Porse et al., 1998). The thiazole rings THZ6 and THZ14 of Thio (**Figure 1A**) stack upon Pro22 and Pro26, respectively, within L11-NTD and therefore mutations, for example, to Ser, Leu or Arg at these positions, or deletion of neighboring residues Ala20-Pro21, could abolish this

type of interaction. More likely is that the mutations have a global (and long-range) influence on the conformation of the L11-NTD by disrupting the proline-rich helix α1, explaining why mutations at Pro23 can also confer resistance, even though this residue does not come within 7 Å of Thio (**Figure 3B**).

Interestingly, in eukaryotic organisms many of the Pro residues are not conserved (**Supplemental Figure 3**), specifically, Pro22, Pro23 and Pro56 are usually Ser, Ala or Thr at the equivalent positions. Since mutations at positions Pro22 and Pro23 (to Ser or Thr) as well as Pro56 (to His) confer resistance to Thio in various bacteria (Cameron et al., 2004), the natural thiopeptide resistance of eukaryotes can be explained by presence of Ser, Ala and Thr at these positions. However, it should be noted that 90-98% of known eukaryotic 23S rRNA sequences also contain a guanine at the position equivalent to *E. coli* A1067 (**Supplemental Figure 2**), and as mentioned above A1067G mutations confer Thio resistance in bacteria and archaea. Thus eukaryotes can be considered to be "doubly" protected through the presence of rRNA as well as protein differences.

Interrelationship between thiostrepton, nosiheptide, L11 and EF-G on the ribosome

We have recently determined a 7.3 Å cryo-EM reconstruction of *T. thermophilus* 70S•EF-G•GDPNP complex (Connell et al., 2007; **Figure 4A** and **B**). The sub-nanometer resolution enables secondary structure elements to be identified in the electron density corresponding to EF-G and r-proteins, which greatly aids the docking of X-ray structures. Of particular interest for this study, the cryo-EM map reveals continuous density between EF-G and components of the stalk base (SB), implying an interaction whereby α-helix A_5 in domain V of EF-G approaches the SB cleft formed by H44, and the β-strand 2_5 potentially interacts with H43 and the proline rich α1 of the L11-NTD (**Figure 4C** and **D**). The latter interaction is consistent with the strong protection of A1067 from DMS probing upon binding of EF-

G•GDPNP to the ribosome (Moazed et al., 1988). Moreover, this is also in agreement with the reported crosslink between EF-G and rRNA in the vicinity of A1067 (Skold, 1983), as well as the dramatic reduction in A1067C mutations have on uncoupled EF-G dependent GTPase activity (Cameron et al., 2002). Additionally, site-directed hydroxyl-radical probing from residues located in domain V of EF-G result in cleavage within the loops of H43 and H44 (Wilson and Noller, 1998).

The mechanism by which thiopeptides inhibit EF-G action can be understood by aligning the D50S-thiopeptide and 70S•EFG•GDPNP structures on the basis of H43 and H44, revealing an extensive overlap between Thio (**Figure 4D**) or Nosi (data not shown) and EF-G. Thio sterically clashes with EF-G by mimicking to some extent regions of domain V, i.e. loop1 of Thio approaches the position of EF-G β-strand 1_5 while loop1 and the QA moiety of loop2 superimpose with the antiparallel EF-G β-strands 2_5 and 3_5, respectively (**Figure 4D**). Additionally the interaction of the tail of Thio/Nosi appears to further fix the position of L11 with respect to the SB. This arrangement of L11 is dramatically different than that seen in the 70S•EFG•GDPNP complex, where EF-G binding seems to displace the L11-NTD so that the cleft widens compared to that seen in the Thio/Nosi structure (**Figure 4D**). In this regard not only would Thio compete with EF-G, but it would lock the L11-NTD in a position such that it also contributes to preventing stable interaction between EF-G and the SB. Figure 4D illustrates that if the L11-NTD were to be fixed as seen in the D50S-thiopeptide structure, then the α1 of L11-NTD would come too close to the β-strand 1_5 of domain V of EF-G. The strong overlap between Thio and EF-G is consistent with reports that Thio abolishes the binding of EF-G to the 70S ribosome (Cameron et al., 2002), as well as more indirect evidence showing that Thio reduces crosslinking of EF-G to the ribosome (for example, see Skold, 1983). A model for the biologically active dehydropiperidine (DHP) core fragment of Thio (inset to **Figure 1A**; Nicolaou et al., 2005) bound to the ribosome, suggests that DHP,

like Thio, also locks the L11-NTD to the rRNA (**Figure 4E**), lending support to the importance of this feature of thiopeptides for their inhibitory action.

Conflicting reports based on fast kinetic and FRET studies, however, indicate that Thio does not inhibit binding or GTP hydrolysis, but instead prevents translocation, Pi release, and multiple turnover by trapping the factor on the ribosome (Pan et al., 2007; Rodnina et al., 1999; Seo et al., 2006). We believe that these results can be reconciled if one considers that Thio does not prevent binding of EF-G *per se*, but precludes formation of a tight complex that can be monitored by centrifugal binding assays (Cameron et al., 2002) while allowing a weak binding that can be detected indirectly by the time-resolved studies (Rodnina et al., 1999; Seo et al., 2006). Indeed, Thio has been demonstrated to produce a 10-fold decrease in EF-G•GDPNP binding to 70S ribosomes by slowing the initial binding and preventing the conversion from a weaker initial complex to a subsequent stable complex (Pan et al., 2007; Seo et al., 2004). The SB has been shown to adopt two positions on the ribosome, the "in" and "out" conformations (Schuwirth et al., 2005), with the inward shift occurring when translation factors, such as EF-G, are loaded onto the ribosome (see Spahn et al., 2004 and references therein). In **Figure 4F**, it can be seen that the overlap between Thio and domain V of EF-G is significantly reduced when Thio is modeled onto the SB adopting an out position on the ribosome. This suggests that the initial weak binding of EF-G may represent a state before the SB has moved inwards and tight interactions are formed between H43/44 and domain V of EF-G. Thio would allow this initial interaction and apparently permits GTPase activation, but by restricting access to the cleft between L11-NTD and H43/44, Thio prevents the conformational changes in the ribosome (i.e. in the SB) and EF-G that are required for translocation.

Micrococcin promotes the L11-L7/L12 interaction

As mentioned above, the density for Micro indicates that the drug does not bind in the same position as Thio/Nosi, being displaced by ~6 Å when compared to Thio (**Figure 5A** and **5B**). In the model, the tail of Micro appears to interact with A1095, but the drug does not seem to approach A1067 to the same extent as Thio/Nosi (**Figure 5B**). This is consistent with the fact that mutations at A1095 confer better resistance to Micro than transversions and transitions at A1067 (Rosendahl and Douthwaite, 1994), and is also in agreement with the observation that Micro enhances the chemical reactivity of A1067, rather than protecting it as Thio does (Egebjerg et al., 1989; Rosendahl and Douthwaite, 1993).

Unlike Thio (and Nosi), Micro has been shown to stimulate uncoupled EF-G-dependent GTPase activity (Cameron et al., 2002; Lentzen et al., 2003). Consistent with these differential effects, a number of differences are apparent in the crystal structures. Firstly, the conformation of Micro-L11 is similar to that of L11 in the native D50S structure, thus the conformational switch observed in the distal region of the L11-NTD, as is observed upon Thio/Nosi binding to the D50S is not induced by Micro. Secondly, additional density appears adjacent to L11-NTD in the D50S-Micro structure, which is not present in the Thio/Nosi structures. This density can be modeled as the CTD of L7/L12 (L7-CTD; residues 52-122), allowing the interaction interface between L11-NTD and L7-CTD to be defined. The interaction surface comprises two main regions of L11-NTD, namely, the loop between β2 and β3 that inserts into a crevice between α4 and α6 of L7-CTD, and the N-terminus of L11, which makes additional contacts to the proximal end of α4 (**Figure 5C**). In the native D50S structure, the density for the L11-NTD is relatively poor due to its apparent flexibility, however the predominant conformation of the NTD appears to be almost identical to Micro-bound L11-NTD and careful re-inspection reveals additional density, albeit weaker, which is consistent with the presence of L7-CTD in the same position as observed in the Micro structure (data not shown). These results suggest that the interaction observed in the Micro-

D50S structure between L11 and L7 is indeed 'physiological' since it also occurs on native ribosomes, and that the presence of Micro stabilizes this interaction. In contrast, the conformational switch introduced in the L11-NTD by Thio/Nosi would prevent the L7-L11 interaction, which likely contributes to the different inhibitory effect of these drugs (**Figure 5D**).

Previous cryo-EM studies on the 70S•EF-G•Fus•GDP complexes (Datta et al., 2005) also support an interaction between L7 and the distal tip of L11-NTD, however, the relative arrangement of L11 and L7 differs from our study (**Supplemental Figure 4**). When aligning the L11-NTD-L7-CTD complex from the Micro-D50S structure to the 70S•EFG•GDPNP cryo-EM reconstruction (Connell et al., 2007), the position of L7-CTD correlates with the fragmented density attributed to L7/L12 in the cryo-EM structure (**Figure 5E**). In this orientation, the α4 and α5 helices of L7-CTD face toward two α-helices, A_G and particularly B_G, located in the G' domain of EF-G. This interaction surface is consistent with the complementarities of these two surfaces in terms of electrostatic potential (**Supplemental Figure 5**), as well as the large number of highly conserved residues that project toward EF-G from the α4-α5 surface of L7-CTD. Moreover, NMR studies implicate many of these conserved residues, namely, Val66-Val68, Lys70, Leu80 and Glu82, in forming direct interaction with EF-G (**Figure 5F**) (Helgstrand et al., 2007), and mutations of residues in helix α4 (Val66, Ile69, Lys70 and Arg73) strongly inhibit Pi release without affecting single turnover GTPase or translocation functions of EF-G (**Figure 5G**) (Savelsbergh et al., 2005).

In accordance with previous biochemical studies (Cameron et al., 2002; Lentzen et al., 2003) we suggest that Micro stimulates the uncoupled GTPase of EF-G by stabilizing the L11-L7 interaction and in doing so pre-positions L7 for interaction with EF-G. Once positioned on EF-G, L7 would stimulate EF-G turnover by promoting Pi release in accordance with fast kinetic studies (Diaconu et al., 2005; Savelsbergh et al., 2005).

Discussion

In this study we used X-ray crystallography to elucidate the binding sites of Thio, Nosi and Micro on the large ribosomal subunit. These results have been further analyzed within the context of a cryo-EM reconstruction of a 70S•EFG•GDPNP complex that we have previously reported (Connell et al., 2007).

A comparison of these structures reveals a critical point on the ribosome in the region of L7 and L11 which adopts different conformations depending on the type of ligand present. Specifically the ligands seem to control two molecular switches in the ribosomal protein L11 which, by changing its conformation on the ribosome, creates different scenarios, as follows:

The first switch in L11, Switch 1 is an inter-domain event analogous to the switch proposed to exist on the basis of the flexibility of the L11-NTD (Porse et al., 1998; Wimberly et al., 1999). Switch 1 involves the displacement of the L11-NTD with respect to the L11-CTD and controls the widening and closure of the cleft present at the SB between the L11-NTD and H43/44 of the rRNA (the switch between the "off" and "on" positions is arrowed in **Figure 4D**). Switch 1 is stabilized in the "on" position upon EF-G binding, such that the open conformation allows proper insertion and accommodation of domain V of EF-G within the cleft of the stalk base (SB) (**Figure 4C**). In contrast, the Thio/Nosi-D50S structures reveal that the drugs, by interacting with both H43/44 and L11-NTD, lock Switch 1 in the "off" position by restricting the L11-NTD movement that leads to cleft widening (**Figure 4D**).

The second switch in L11, Switch 2, is an intra-domain event that involves a conformational change within L11-NTD, such that in the "on" position, a complementary surface is formed to promote a stable interaction between L11-NTD and L7-CTD (**Figure 5D**). Switch 2 is observed in the "off" position in the presence of Thio and Nosi, while with Micro and in the 70S•EFG•GDPNP complex, Switch 2 is in the "on" position. In the latter case, the interaction between the L11-NTD with the L7-CTD positions the L7-CTD in close contact with the G' domain of EF-G (**Figure 5E** and **Supplemental Figure 5**).

When these results are taken within the context of our current knowledge of the elongation cycle, it is possible to revisit the sequence of events controlled and triggered on the ribosome by EF-G. Figure 6 provides a model for the role played by the two molecular switches identified in L11 as well as rationalizing the specific inhibitory effects of the thiopeptide class of antibiotics. The details of the model are as follows:

Cryo-EM reconstructions (Frank and Agrawal, 2001; Li et al., 2006; Spahn et al., 2004; Valle et al., 2003) reveal that as elongation factors are loaded onto the ribosome, the SB oscillates between "out" and "in" positions (**Figure 6A** and **B**). In the case of EF-G, this transition is accompanied by the hydrolysis of GTP which has been shown to occur as soon as EF-G interacts with the ribosome (**Figure 6A**) - in contrast to the release of inorganic phosphate (Pi) and translocation, which are much slower steps (Rodnina et al., 1999; Seo et al., 2004; Savelsbergh et al., 2005; Seo et al., 2006), facilitated by the involvement of L7/L12 (Savelsbergh et al., 2005). In this respect, the activation of both molecular switches identified in L11 play an important role: Firstly, turning "on" Switch 1 ensures the proper insertion and accommodation of domain V of EF-G into the widened cleft present at the SB (**Figure 6B**), and secondly, Switch 2 promotes a stable interaction of the L7-CTD with the L11-NTD, such that L7-CTD is optimally positioned to contact the G' domain of EF-G (**Figure 6C**). L7 has been shown to be important for stimulating Pi release, but not GTP hydrolysis *per se* (Savelsbergh et al., 2005), suggesting that the interaction of the L7-CTD with the G' domain of EF-G will trigger conformational changes within the GTP-binding pocket of EF-G to allow Pi release (**Figure 6D**).

In the model described above, Thio and Nosi seem to interfere at two different levels:, First of all the Thiopeptide-D50S structures reveal that the drugs, by interacting with both H43/44 and L11-NTD, block the Switch 1 event in L11 (**Figure 6B**) by restricting the L11-NTD movement that leads to the widening of the cleft and thus prevent EF-G from entering the cleft and stably interacting with the SB (**Figure 6E**). This is consistent with the more

labile initial binding state of EF-G on the ribosome observed in the presence of Thio (Seo et al., 2006). Moreover, the structure of Thio/Nosi bound to the D50S reveal that these drugs also interfere with EF-G action at the Switch 2 level; both Thio and Nosi stabilize the structure of the L11-NTD in the "off" position, i.e. inducing a conformational change within the L11-NTD that perturbs the L11-L7 interaction surface. This in turn prevents binding of L7-CTD to L11 (**Figure 6E**), thus explaining the reduction in Pi release observed in the presence of these drugs (Cameron et al., 2002; Lentzen et al., 2003; Rodnina et al., 1999; Seo et al., 2006; Seo et al., 2004).

In contrast to Thio and Nosi, Micro has been shown to stimulate, rather than inhibit, the uncoupled EF-G dependent GTPase activity of the ribosome (Cameron et al., 2002; Lentzen et al., 2003). Accordingly, in the crystal structure of the large ribosomal subunit in complex with Micro, we observe a different situation, in which, Micro (i) displays a different interaction with rRNA of the SB, although it would still prevent the Switch 1 event by restricting the inter-domain movement in L11, (ii) fails to invoke the intra-domain conformational changes seen within the L11-NTD of the Thio/Nosi structures, but instead (iii) turns Switch 2 "on" by promoting or stabilizing the interaction between L11 and L7-CTD (**Figure 6F**). Micro may therefore function to stimulate the uncoupled GTPase of EF-G by stabilizing the L11-L7 interaction and thus pre-positioning L7 on L11 so that it can interact with EF-G. Once positioned on EF-G, L7 would constantly stimulate GTP turnover by promoting Pi release in accordance with biochemical studies (Cameron et al., 2002). This indicates that turning Switch 2 "on" can occur independently of Switch 1 activation, and does so at least in the case of Micro.

Therefore, we suggest that the double-switching mechanism identified in L11 acts as a molecular sensor to monitor and control the translational state of the ribosome, allowing the functional complex to move from the labile initial binding state of EF-G to its stable accommodated state and then forward to the low-affinity EF-G dissociation state that occurs

upon Pi release. The presence and conservation of the two domains structure of L11 throughout all kingdoms of life suggests that this double-switching mechanism may be universal.

Experimental Procedures

Crystallography

D. radiodurans large ribosomal subunit crystals were prepared as described (Schlünzen et al., 2001), and soaked in a cryo-solution containing 20-40 μM thiopeptide (Thio, Micro or Nosi) for 12-24 hrs, prior to freezing. Data were collected at 100K from shock frozen crystals at X06SA at Swiss Light Source (SLS), Villigen, Switzerland. Data were recorded on MAR345 or Quantum 4 detectors and processed with HKL2000 (Otwinowski and Minor, 1997) and the CCP4 package (Bailey, 1994).

Modeling and Docking:

The native structure of the D50S subunit (Wilson et al., 2005 and pdb3xxx) was refined against the structure factor amplitudes of the D50S-thiopeptide antibiotic complexes, using rigid body refinement as implemented in CNS (Brunger et al., 1998). For the calculation of the free R-factor, 5% of the data were omitted during refinement. The position of the Thiazole antibiotics, H43, H44, L11 and L12-CTD were determined from sigma-weighted difference maps or composite omit maps followed by density modification and phase recombination as described in Diaconu et al., 2005. Further refinement was carried out using CNS (see **Supplemental Table 1** for refinement statistics).

The D50S-thiopeptide antibiotic interactions were originally determined with Chimera (Pettersen et al., 2004). Alignment of the EF-G•GDPNP•70S complex (Connell et al., 2007) and the Thio-SB model (pdb1OLN; Lentzen et al., 2003) were performed by least square alignments of H43-44 onto the D50S structure (Harms et al., 2001). The starting model for

refinement of the L7-CTD was based on a homology model for *D. radiodurans* L7-CTD generated using the Protein Homology/analogY Recognition Engine (PHYRE) (http://www.sbg.bio.ic.ac.uk/~phyre/) with the crystal structure for *T. maritima* L7 (PDB1DD3; Wahl et al., 2000) as a template. Electrostatic potentials were calculated using the program APBS (Baker et al., 2001) and buried surface area with AREAIMOL in the CCP4 package (Bailey, 1994).

Coordinates and Figures

All crystallographic figures were produced using PyMol (http://www.pymol.org). Final coordinates and structure factors for native-D50S, Thio-D50S, Nosi-D50S and L7-CTD-D50S (Micro) have been deposited in the Protein Data Bank under accession number 3xxx, 3xxx, 3xxx and 3xxx, respectively.

Acknowledgments

We would like to thank Renate Albrecht, Joerg Buerger and Barbara Schmidt for helpful technical assistance, Profs Cooperman, Schwalbe and Wöhnert as well as Dr. Jonker for fruitful discussions, Prof. Floss for providing us with the antibiotic nosiheptide, and Prof. Joseph Puglisi and Dr. Andy Marshall for help accessing the small molecule structure of nosiheptide. These studies could not have been performed without the expert assistance of the staff, in particular Dr. Takashi Tomazaki and Dr. Clemens Schulze-Briese, at the synchrotron facilities X06SA/SLS and Dr. Joanne McCarthy, at the synchrotron facilities ID29/ESRF. Support for this work was provided by the Deutsche Forschungsgemeinschaft (FU579 1-3 to P.F. and WI3285/1-1 to D.W.). P.F. is supported by the Cluster of Excellence "Macromolecular Complexes" at the Goethe University Frankfurt (DFG Project EXC 115)".

References

Bailey, S. (1994). The *CCP*4 suite: programs for protein crystallography. Collaborative Computational Project, Number 4. Acta Crystallographica D Biol Crystallogr. *50*, 760-763.

Baker, N., Sept, D., Joseph, S., Holst, M., and McCammon, J. (2001). Electrostatics of nanosystems: application to microtubules and the ribosome. Proc. Natl Acad. Sci. USA *98*, 10037-10041.

Ban, N., Nissen, P., Hansen, J., Moore, P. B., and Steitz, T. A. (2000). The complete atomic structure of the large ribosomal subunit at 2.4 Å resolution. Science *289*, 905-920.

Bausch, S., Poliakova, E., and Draper, D. (2005). Interactions of the N-terminal domain of ribosomal protein L11 with thiostrepton and rRNA. J. Biol. Chem. *280*, 29956-29963.

Bond, C., Shaw, M., Alphey, M., and Hunter, W. (2001). Structure of the macrocycle thiostrepton solved using the anomalous dispersion contribution of sulfur. Acta crystallographica D Biol Crystallogr. *57*, 755-758.

Bowen, W., Van Dyke, N., Murgola, E., Lodmell, J., and Hill, W. (2005). Interaction of thiostrepton and elongation factor-G with the ribosomal protein L11-binding domain. J. Biol. Chem. *280*, 2934-2943.

Brunger, A., Adams, P., Clore, G., DeLano, W., Gros, P., Grosse-Kunstleve, R., Jiang, J., Kuszewski, J., Nilges, M., Pannu, N., *et al.* (1998). Crystallography & NMR system: A new software suite for macromolecular structure determination. Acta Crystallogr. D Biol. Crystallogr. *54*, 905-921.

Cameron, D., Thompson, J., Gregory, S., March, P., and Dahlberg, A. (2004). Thiostrepton-resistant mutants of *Thermus thermophilus*. Nucleic Acids Res. *32*, 3220-3227.

Cameron, D. M., Thompson, J., March, P. E., and Dahlberg, A. E. (2002). Initiation factor IF2, thiostrepton and micrococcin prevent the binding of elongation factor G to the *Escherichia coli* ribosome. J. Mol. Biol. *319*, 27-35.

Connell, S. R., Takemoto, C., Wilson, D. N., Wang, H., Murayama, K., Terada, T., Shirouzu, M., Rost, M., Schuler, M., Giesebrecht, J., *et al.* (2007). Structural basis for interaction of the ribosome with the switch regions of GTP-bound elongation factors. Mol. Cell *25*, 751-764.

Cundliffe, E., Dixon, P., Stark, M., Stöffler, G., Ehrlich, R., Stöffler-Meilicke, M., and Cannon, M. (1979). Ribosomes in thiostrepton-resistant mutants of *B. megaterium* lacking a single 50S subunit protein. J. Mol. Biol. *132*, 235-252.

Datta, P. P., Sharma, M. R., Qi, L., Frank, J., and Agrawal, R. K. (2005). Interaction of the G' domain of elongation factor G and the C-terminal domain of ribosomal protein L7/L12 during translocation as revealed by cryo-EM. Mol. Cell *20*, 723-731.

Diaconu, M., Kothe, U., Schlunzen, F., Fischer, N., Harms, J. M., Tonevitsky, A. G., Stark, H., Rodnina, M. V., and Wahl, M. C. (2005). Structural basis for the function of the ribosomal L7/12 stalk in factor binding and GTPase activation. Cell *121*, 991-1004.

Egebjerg, J., Douthwaite, S., and Garrett, R. A. (1989). Antibiotic interactions at the GTPase associated centre within *Escherichia coli* 23S rRNA. EMBO J. *8*, 607-611.

Frank, J., and Agrawal, R. (2001). Ratchet-like movements between the two ribosomal subunits: their implications in elongation factor recognition and tRNA translocation. Cold Spring Harb. Symp. Quant. Biol. *66*, 67-75.

Hansen, J. L., Ippolito, J. A., Ban, N., Nissen, P., Moore, P. B., and Steitz, T. A. (2002). The structures of four macrolide antibiotics bound to the large ribosomal subunit. Mol. Cell *10*, 117-128.

Harms, J., Schluenzen, F., Zarivach, R., Bashan, A., Gat, S., Agmon, I., Bartels, H., Franceschi, F., and Yonath, A. (2001). High resolution structure of the large ribosomal subunit from a mesophilic eubacterium. Cell *107*, 679-688.

Helgstrand, M., Mandava, C. S., Mulder, F. A., Liljas, A., Sanyal, S., and Akke, M. (2007). The ribosomal stalk binds to translation factors IF2, EF-Tu, EF-G and RF3 via a conserved region of the L12 C-terminal domain. J. Mol. Biol. *365*, 468-479.

Highland, J. H., and Howard, G. A. (1975). Assembly of ribosomal proteins L7, L10, L11 and L12 on the 50S subunit of *E. coli*. J. Biol. Chem. *250*, 831-834.

Hummel, H., and Boeck, A. (1987). Thiostrepton resistance mutations in the gene for 23S ribosomal RNA of halobacteria. Biochimie *69*, 857-861.

Jonker, H. R., Ilin, S., Grimm S. K., Wöhnert, J., Schwalbe, H. (2007) L11 domain rearrangement upon binding to RNA and thiostrepton studied by NMR spectroscopy. Nucleic Acids Res. *35*, 441-454.

Lentzen, G., Klinck, R., Matassova, N., Aboul-ela, F., and Murchie, A. (2003). Structural basis for contrasting activities of ribosome binding thiazole antibiotics. Chem. Biol. *10*, 769-778.

Li, W., Sengupta, J., Rath, B. K., and Frank, J. (2006). Functional conformations of the L11-ribosomal RNA complex revealed by correlative analysis of cryo-EM and molecular dynamics simulations. RNA *12*, 1-14.

Mankin, A. S., Leviev, I., and Garrett, R. A. (1994). Cross-hypersensitivity effects of mutations in 23 S rRNA yield insight into aminoacyl-tRNA binding. J. Mol. Biol. *244*, 151-157.

Moazed, D., Robertson, J. M., and Noller, H. F. (1988). Interaction of elongation factors EF-G and EF-Tu with a conserved loop in 23S RNA. Nature *334*, 362-364.

Nicolaou, K., Zak, M., Rahimipour, S., Estrada, A., Lee, S., O'Brate, A., Giannakakou, P., and Ghadiri, M. (2005a). Discovery of a biologically active thiostrepton fragment. J. Am. Chem. Soc. *127*, 15042-15044.

Nicolaou, K., Zak, M., Safina, M., Estrada, A., Lee, S., and Nevalainen, M. (2005b). Total synthesis of thiostrepton. Assembly of key building blocks and completion of the synthesis. J. Am. Chem. Soc. *127*, 11176-11183.

Otwinowski, Z., and Minor, W. (1997). Processing of X-ray diffraction data collected in oscillation mode. Methods Enzymol. *276*, 307-326.

Pan, D., Kirillov, S. V., and Cooperman, B. S. (2007). Kinetically competent intermediates in the translocation step of protein synthesis. Mol. Cell *25*, 519-529.

Pettersen, E. F., Goddard, T. D., Huang, C. C., Couch, G. S., Greenblatt, D. M., Meng, E. C., and Ferrin, T. E. (2004). UCSF Chimera - A Visualization System for Exploratory Research and Analysis. J. Comput. Chem. *25*, 1605-1612.

Porse, B. T., Cundliffe, E., and Garrett, R. A. (1999). The antibiotic micrococcin acts on protein L11 at the ribosomal GTPase centre. J. Mol. Biol. *287*, 33-45.

Porse, B. T., Leviev, I., Mankin, A. S., and Garrett, R. A. (1998). The antibiotic thiostrepon inhibits a functional transition within protein L11 at the ribosomal GTPase centre. J. Mol. Biol. *276*, 391-404.

Prange, T., Ducruix, A., Pascard, C., and Lunel, J. (1977). Structure of nosiheptide, a polythiazole-containing antibiotic. Nature *265*, 189-190.

Rodnina, M. V., Savelsbergh, A., Matassova, N. B., Katunin, V. I., Semenkov, Y. P., and Wintermeyer, W. (1999). Thiostrepton inhibits the turnover but not the GTPase of elongation factor G on the ribosome. Proc. Natl Acad. Sci. USA *96*, 9586-9590.

Rogers, M. J., Cundliffe, E., and McCutchan, T. F. (1998). The antibiotic micrococcin is a potent inhibitor of growth and protein synthesis in the malaria parasite. Antimicrob Agents Chemother. *42*, 715-716.

Rosendahl, G., and Douthwaite, S. (1993). Ribosomal proteins L11 and L10.$(L12)_4$ and the antibiotic thiostrepton interact with overlapping regions of the 23S rRNA backbone in the ribosomal GTPase centre. J. Mol. Biol. *234*, 1013-1020.

Rosendahl, G., and Douthwaite, S. (1994). The antibiotics micrococcin and thiostrepton interact directly with 23S rRNA nucleotides 1067A and 1095A. Nucleic Acids Res. *22*, 357-363.

Savelsbergh, A., Mohr, D., Kothe, U., Wintermeyer, W., and Rodnina, M. V. (2005). Control of phosphate release from elongation factor G by ribosomal protein L7/12. EMBO J. *24*, 4316–4323.

Schlünzen, F., Zarivach, R., Harms, J., Bashan, A., Tocilj, A., Albrecht, R., Yonath, A., and Franceschi, F. (2001). Structural basis for the interaction of antibiotics with the peptidyl transferase centre in eubacteria. Nature *413*, 814-821.

Schuwirth, B., Borovinskaya, M., Hau, C., Zhang, W., Vila-Sanjurjo, A., Holton, J., and Cate, J. (2005). Structures of the bacterial ribosome at 3.5 Å resolution. Science *310*, 827-834.

Seo, H., Abedin, S., Kamp, D., Wilson, D. N., Nierhaus, K. H., and Cooperman, B. S. (2006). EF-G-dependent GTPase on the ribosome. Conformational change and fusidic acid inhibition. Biochemistry *45*, 2504-2514.

Seo, H., Kiel, M., Pan, D., Raj, V., Kaji, A., and Cooperman, B. S. (2004). Kinetics and thermodynamics of RRF, EF-G, and thiostrepton interaction on the *Escherichia coli* ribosome. Biochemistry *43*, 12728-12740.

Skold, S.-E. (1983). Chemical crosslinking of EF-G to 23S RNA in 70S ribosomes from *E. coli*. Nucleic Acids Res. *11*, 4923-4932.

Spahn, C. M., Gomez-Lorenzo, M. G., Grassucci, R. A., Jorgensen, R., Andersen, G. R., Beckmann, R., Penczek, P. A., Ballesta, J. P., and Frank, J. (2004). Domain movements of elongation factor eEF2 and the eukaryotic 80S ribosome facilitate tRNA translocation. EMBO J. *23*, 1008-1019.

Spahn, C. M. T., and Prescott, C. D. (1996). Throwing a spanner in the works: antibiotics and the translational apparatus. J. Mol. Med. *74*, 423-439.

Thompson, J., Cundliffe, E., and Dahlberg, A. E. (1988). Site-directed mutagenesis of *Escherichia coli* 23S ribosomal RNA at position 1067 within the GTP hydrolysis center. J. Mol. Biol. *203*, 457-465.

Thompson, J., Cundliffe, E., and Stark, M. (1979). Binding of thiostrepton to a complex of 23S rRNA with ribosomal protein L11. Eur. J. Biochem. *98*, 261-265.

Thompson, J., Schmidt, F., and Cundliffe, E. (1982). Site of action of a ribosomal RNA methylase conferring resistance to thiostrepton. J. Biol. Chem. *257*, 7915-7917.

Valle, M., Zavialov, A., Li, W., Stagg, S. M., Sengupta, J., Nielsen, R. C., Nissen, P., Harvey, S. C., Ehrenberg, M., and Frank, J. (2003). Incorporation of aminoacyl-tRNA into the ribosome as seen by cryo-electron microscopy. Nat. Struct. Biol. *10*, 899-906.

Wahl, M., Bourenkov, G., Bartunik, H., and Huber, R. (2000). Flexibility, conformational diversity and two dimerization modes in complexes of ribosomal protein L12. EMBO J. *19*, 174-186.

Wienen, B., Ehrlich, R., Stoffler-Meilicke, M., Stoffler, G., Smith, I., Weiss, D., Vince, R., and Pestka, S. (1979). Ribosomal protein alterations in thiostrepton- and micrococcin-resistant mutants of *Bacillus subtilis.* J. Biol. Chem. *254*, 8031-8041.

Wilson, D. N., and Nierhaus, K. H. (2005). Ribosomal Proteins in the Spotlight. Crit. Rev. Biochem. Mol. Biol. *40*, 243-267.

Wilson, D. N., Harms, J. M., Nierhaus, K. H., Schlünzen, F., Fucini, P. (2005). Species-specific antibiotic-ribosome interactions: implications for drug development. Biol. Chem. *386*, 1239-1252.

Wilson, D. N. (2004). Antibiotics and the inhibition of ribosome function. In Protein Synthesis and Ribosome Structure, K. H. Nierhaus, and D. N. Wilson, eds. (Weinheim, Wiley-VCH), pp. 449-527.

Wilson, K. S., and Noller, H. F. (1998). Mapping the position of translational elongation factor EF-G in the ribosome by directed hydroxyl radical probing. Cell *92*, 131-139.

Wimberly, B. T., Guymon, R., McCutcheon, J. P., White, S. W., and Ramakrishnan, V. (1999). A detailed view of a ribosomal active site: The structure of the L11-RNA complex. Cell *97*, 491-502.

Xing, Y. Y., and Draper, D. E. (1996). Cooperative interactions of RNA and thiostrepton antibiotic with two domains of ribosomal protein L11. Biochemistry *35*, 1581-1588.

Figure Legends

Figure 1. Chemical structures of thiopeptide antibiotics

(A) Chemical structure of thiostrepton separated into loops 1 (cyan), 2 (green) and the dehydroalanine (DHA) tail (magenta) linked together by a tetrahydro-pyridin-3-ylamine (TPY; orange) moiety. The 16 distinct chemical moieties are separated by a black bars and are abbreviated as follows: THZ, thiazole-2-carbaldehyde; THR, threonine; DHB, dehydrobutyrine; THF, thiostreptine fragment; THA, thiostreptoic acid; QA, quinaldic acid; ILE, isoleucine; ALA, alanine; PA, pyruvic acid; DHA, dehydroalanine. The boxed inset shows the dehydropiperidine (DHP) core of thiostrepton. Schematic modified from Bond et al. (2001).

(B) Chemical structure of nosiheptide, highlighting the loops 1 (cyan), 2 (green) and tail (magenta).

(C) Chemical structure of micrococcin P1 with loop1 (cyan) and tail (magenta).

Figure 2. Binding position of thiostrepton and nosiheptide on the 50S subunit

(A) Overview of thiopeptide binding site on the *D. radiodurans* 50S subunit. Interface view of the 50S subunit (rRNA and r-proteins coloured light and dark blue respectively) with the thiopeptide binding site boxed. Enlargement of boxed region reveals that the thiopeptides thiostrepton (Thio, cyan) and nosiheptide (Nosi, green) bind within a cleft between the N-terminal domain (NTD) of r-protein L11 (yellow) and the 23S rRNA H43 and H44 (orange).

(B) and (C) 2mFo-DFc σ_A-weighted difference electron density maps (meshed) contoured to 2σ with (B) thiostrepton (Thio), (C) nosiheptide (Nosi), L11-NTD and H44 coloured as in (A).

Figure 3. Interaction of thiostrepton with the ribosome

(A) Stacking and hydrophobic interactions of thiazole (THZ) and quinaldic acid (QA) moieties thiostrepton (Thio, cyan) with bases A1095 (H44) and A1067 (H43) of the 23S rRNA (orange) and proline residues (Pro22 and 26) in L11 (yellow).

(B) Thiostrepton resistance derives from 2'-O-methylation of ribose of A1067 as well as mutations of Pro residues in L11-NTD. The 2'O of A1067 is within 3-4 Å of THZ4 and THF5, whereas Pro23 is >7 Å from any part of the thiostrepton molecule.

(C) Comparison of the free and bound forms of thiostrepton. Docking the small molecule structure of thiostrepton (PDB1E9W; Bond et al., 2001) to the Thio-D50S structure on the basis of aligning loop1, reveals that the tail shifts (as indicated by the arrow) from solvent exposed in the free form (magenta) to contacting L11 in the bound form (cyan).

(D) Conformational change in L11 upon thiostrepton binding. A shift (arrowed) in the distal portion of L11 is seen when comparing the native L11 (Nat-L11; yellow) and thiostrepton bound form of L11 (Thio-L11; cyan).

(E) Comparison of L11 in thiostrepton- and nosiheptide-bound D50S structures. Similar conformations of the L11-NTD are induced by the binding of nosiheptide (Nosi; green) and thiostrepton (Thio; cyan).

Figure 4. Inhibition of L11-EFG interaction by thiostrepton

(A) The cryo-EM reconstruction of the EF-G•GDPNP•70S complex viewed from solvent side of the 30S subunit (Connell et al., 2007), with fitted crystal structures for EF-G (green; PDB1FMN), L7-CTD (magenta) and D50S L11 (yellow). The cryo-EM density (grey surface) has been low-pass filtered to 12 Å to strengthen features, such as the stalk and the L11-NTD, which are disordered in the cryo-EM map at 7.3 Å. However, the shown molecular models were docked into the cryo-EM map at full resolution.

(B) Cryo-EM density as in (A) but with 30S, 50S and EF-G coloured yellow, blue and green, respectively.

(C) Enlargement of (A) showing the interaction of EF-G (green; PDB1FMN) with the stalk base (L11, yellow; H43/44, orange).

(D) Steric clash between thiostrepton and EF-G. Aligning the Thio-D50S and EF-G•GDPNP•70S structures on the basis of H43 and H44, reveals that thiostrepton (Thio, cyan) overlaps significantly with the position of EF-G domain V. Furthermore, the position of the L11-NTD is much more open in the EF-G structure (EFG-L11; yellow) compared to the Thio-D50S position (Thio-L11; cyan).

(E) Model for interaction of dehydropiperidine (DHP) with the ribosome based on the alignment of the analogous moieties of thiostrepton. The thiazole THZ1 and THZ14 moieties are predicted to interact with the base of A1095 in H44 of the 23S rRNA (orange) and with proline 26 (Pro26) in the L11-NTD (yellow).

(F) Thiostrepton allows initial binding of EF-G. The position of thiostrepton (Thio, cyan) modeled on the EF-G•GDPNP•70S structure with the stalk base (SB) in the "out" position reveals only a modest overlap with domain V of EF-G (green). The SB "in" position (transparent) is also included for reference. The SB "out" position was obtained by aligning the appropriate *Escherichia coli* 70S structure (PDB2AWB; Schuwirth et al., 2005).

Figure 5. Interplay between L11, L7/L12 and EF-G on the ribosome

(A) 2mFo-DFc σ_A-weighted difference electron density maps (meshed) contoured to 2σ with micrococcin (Micro), L11-NTD (yellow) and nucleotides A1067, A1068 (H43) and A1095 (H44) of the 23S rRNA (orange) shown. A tentative model for Micro was generated with CORINNA and is shown in blue.

(B) Comparison of the overall positions of micrococcin and thiostrepton. Micro (blue) is displaced away from A1067 in H43 compared to Thio (cyan). In addition, the tail of Micro does not appear to approach the N-terminus of L11, unlike the tail of Thio.

(C) Micrococcin stabilizes the interaction between L11-NTD and L7-CTD. A 2mFo-DFc σ_A-weighted difference electron density map (meshed) contoured to 2σ, reveals that in the presence of micrococcin (Micro; blue), additional density adjacent and interacting with L11 (yellow) can be modeled with the L7-CTD (magenta; PDB1DD3; Wahl et al., 2000). In particular the density allows accurate placement of α4, α5 and α6 of L7-CTD.

(D) Comparison of the conformations of L11 bound to different thiopeptides with respect to L7-CTD. The L11-NTD bound with thiostrepton (Thio-L11; cyan), nosiheptide (Nosi-L11; green) and micrococcin (Micro-L11; yellow) were aligned on the basis of H43 and H44. Unlike Micro, Thio and Nosi induce conformational change in L11-NTD that leads to sterical clashing between the N-terminus of L11 and α4 of L7-CTD.

(E) The relative positions of the L11-L7 complex with respect to EF-G. The L7-L11 (L7, magenta; L11, yellow) complex from the Micro-D50S structure was aligned to the cryo-EM reconstruction of the EF-G•GDPNP•70S map (Connell et al., 2007) using the L11-NTD. L11-NTD, L7-CTD and EF-G from the cryo-EM structure are shown in orange, blue and green, respectively, with cryo-EM density in grey filtered to 14 Å.

(F) and (G) The L7-CTD interacts with the G' domain of EF-G. The orientation and position of L7-CTD is consistent with (F) NMR studies implicating many conserved residues in helix α4 and α5 (green sticks) of L7-CTD as interaction partners for EF-G (Helgstrand et al., 2007), as well as (G) mutations of residues in helix α4 (pink sticks) that strongly inhibit Pi release without affecting single turnover GTPase or translocation functions of EF-G (Savelsbergh et al., 2005).

Figure 6. Schematic for EF-G and thiopeptide action during translation

(A)-(D) Model for events leading to EF-G accommodation on the ribosome and Pi release as described in the text. Effect of (E) Thio (purple) and (F) Micro (brown) are also shown schematically. Individual domains of EF-G are indicated II-V and G/G' domains, (orange) as well as the stalk base (SB) components, L11 (green) with N- and C-terminal domains (NTD, CTD) and rRNA H43 and H44 (blue), and L7-CTD (red). Note for simplicity, the switching mechanism has been divided into two distinct steps, however it is unclear as to whether they are sequential, as shown here, or occur simultaneously.

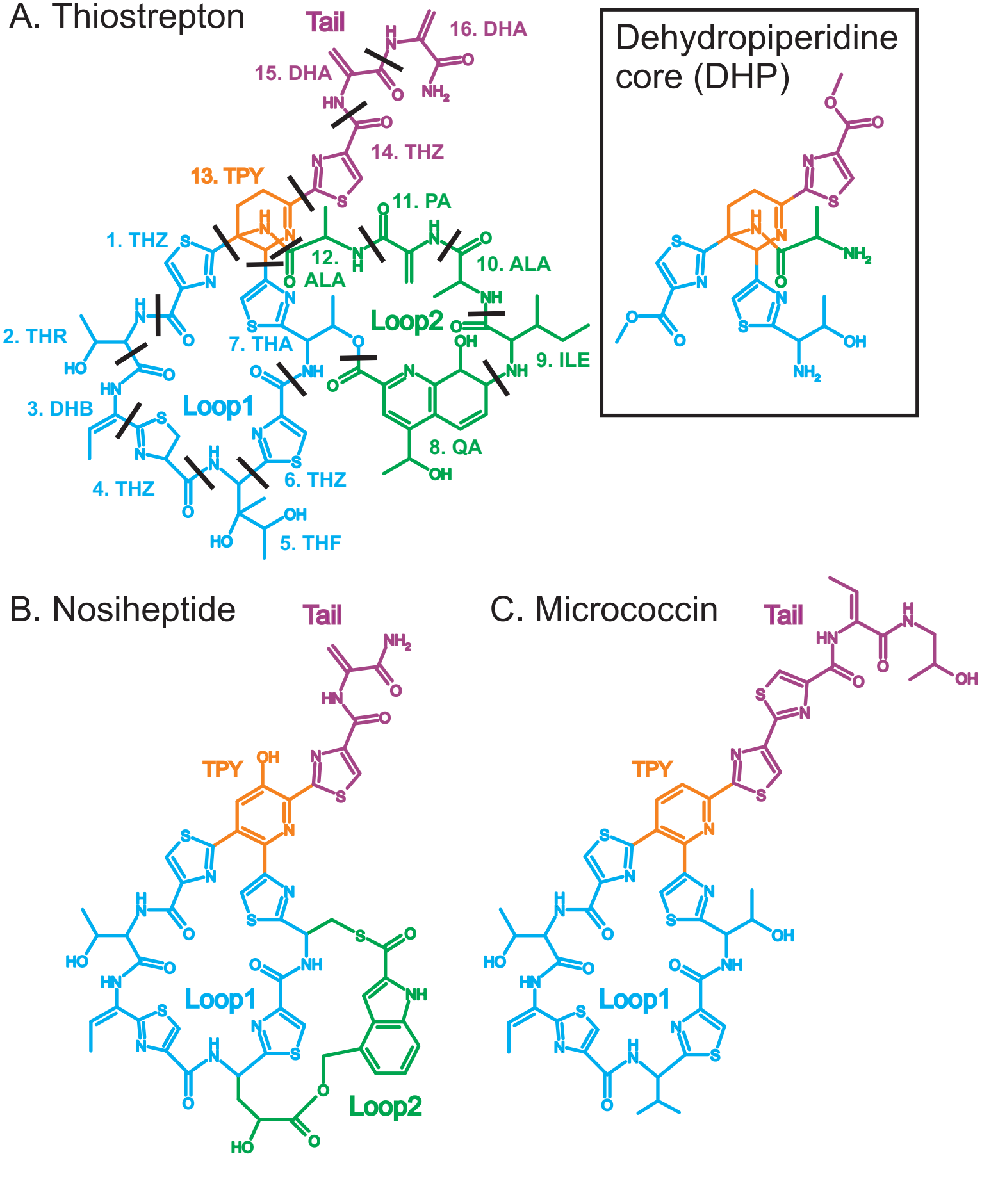

Harms et al Figure 1

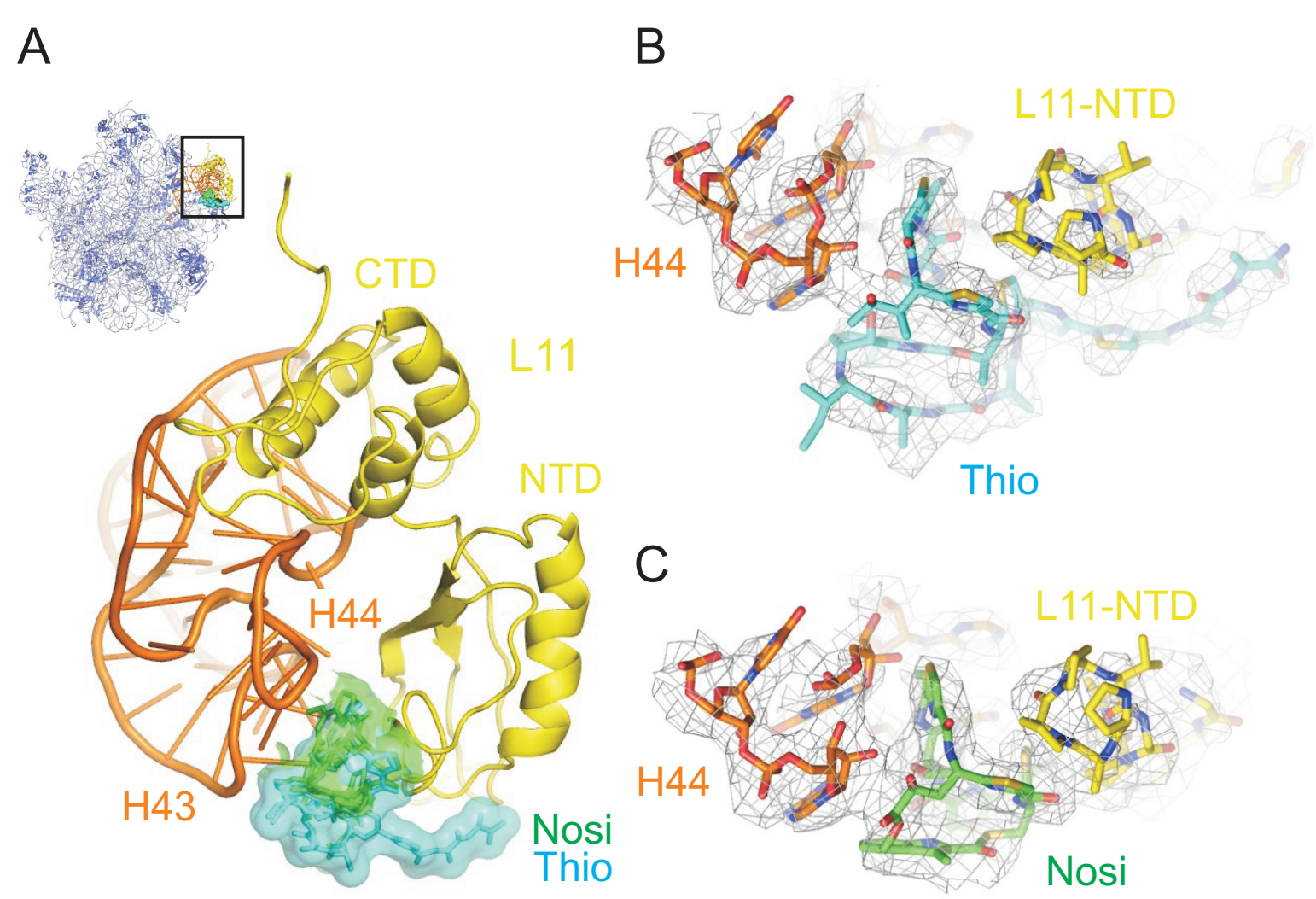

Harms et al Figure 2

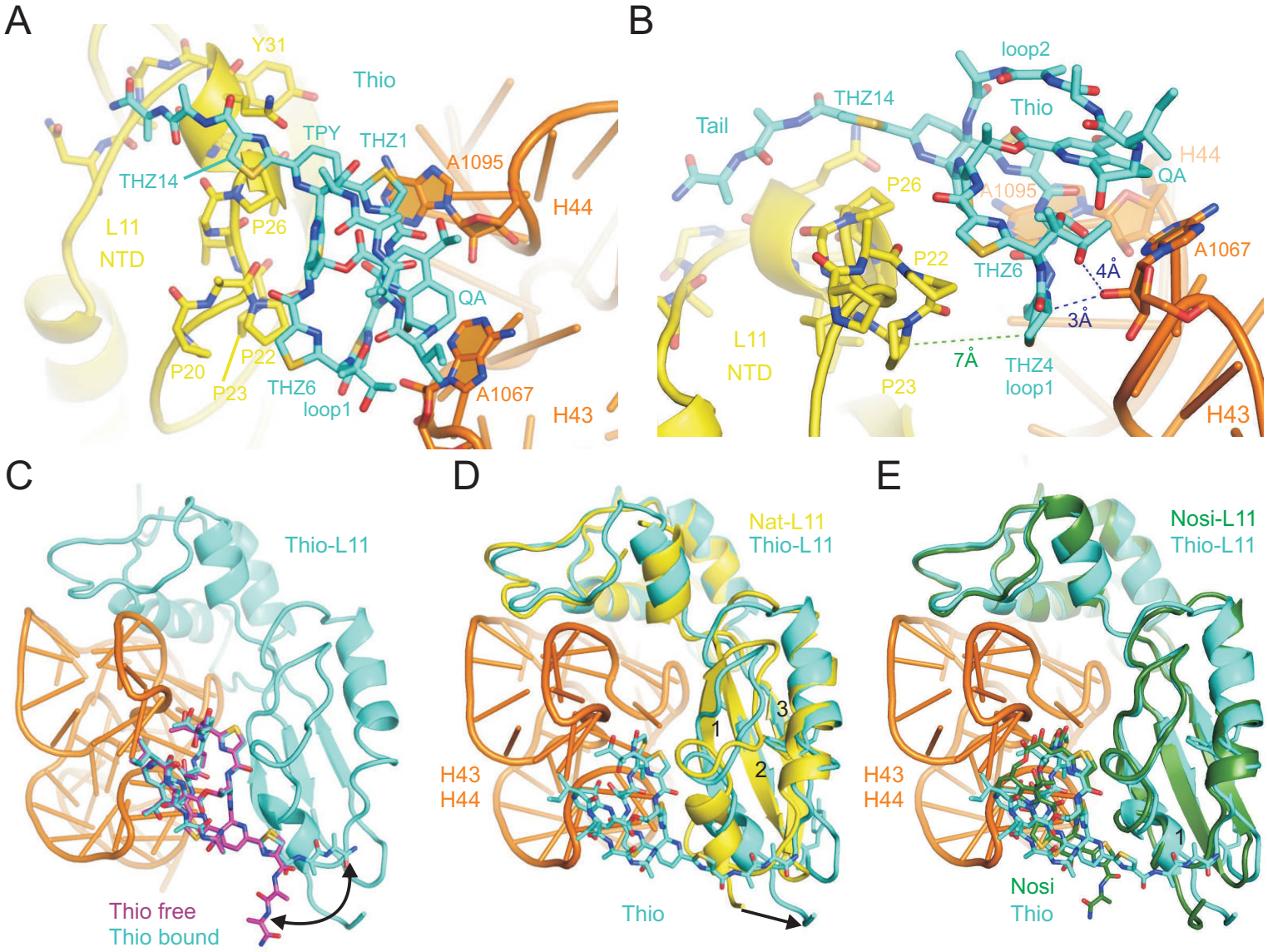

Harms et al Figure 3

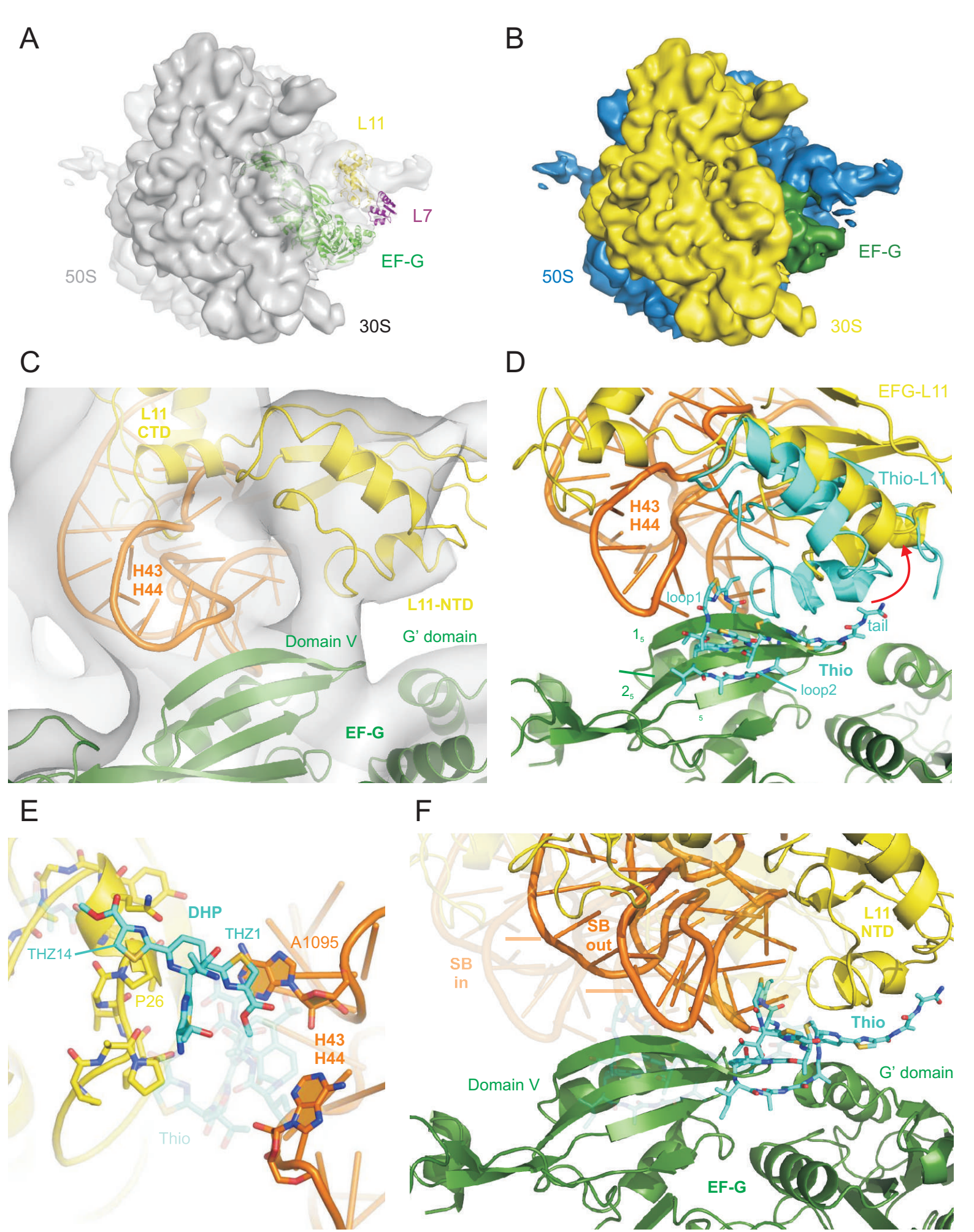

Harms et al Figure 4

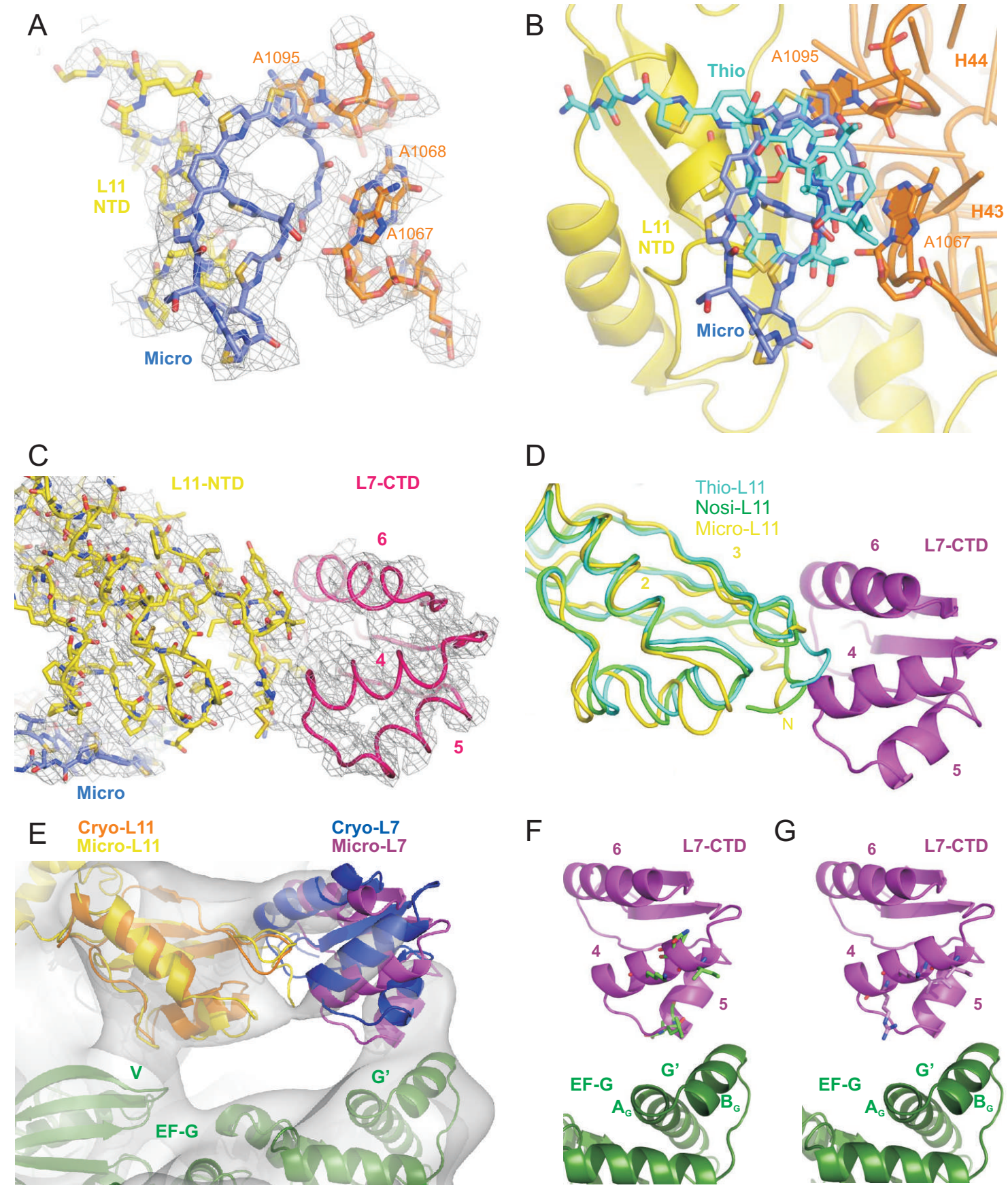

Harms et al Figure 5

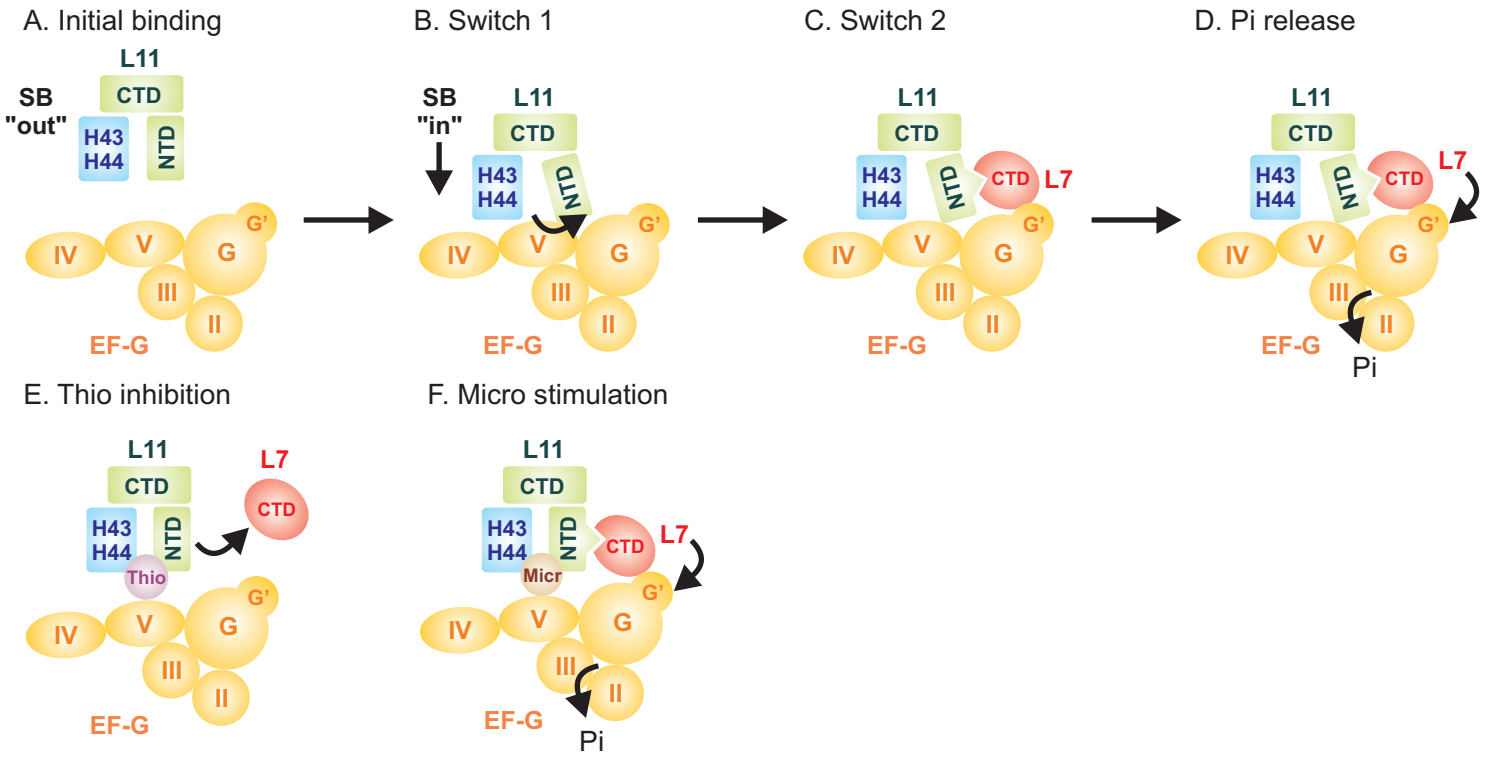

Harms et al Figure 6

Supplemental Data

Table 1

Crystallography data collection and refinement statistics

Crystal Information :		Space group I222	
	D50-Micrococcin	**D50-Nosiheptide**	**D50-Thiostrepton**
Unit cell dimensions (Å)	169.7x410.6x695.0	169.9x408.9x694.5	169.4x408.6x693.8
Resolution (Å)	30-3.3 (3.36-3.30)	30-3.7 (3.76-3.70)	50-3.3 (3.36-3.30)
Number of unique reflections	352577	216249	342617
Completeness (%)	97.8 (89.0)	85.6 (75.2)	94.1 (84.1)
R_{sym} (%)	13.3 (62.1)	14.0 (63.0)	16.4 (49.1)
Mean I/s(I)	7.5(1.3)	6.1(1.2)	5.3(1.3)
Refinement statistics			
R factor (%)	0.3016	0.2997	0.2760
R_{free} (%)	0.3386	0.3395	0.3182
RMS deviations from ideal geometry			
Bond length	0.010592	0.009426	0.010155
Bond angles	1.54328	1.47416	1.55318
Ramachandran for L11 [L12]			
Residues in most favored or additional allowed regions	113 (97.4%) [61 (100%)]	111 (95.7%)	108 (93.1%)
Residues in generously allowed regions	2 (1.7%) [0 (0%)]	3 (2.6%)	7 (6.0%)
Residues in disallowed regions	1 (0.9%) [0 (0%)]	2 (1.7%)	1 (0.9%)

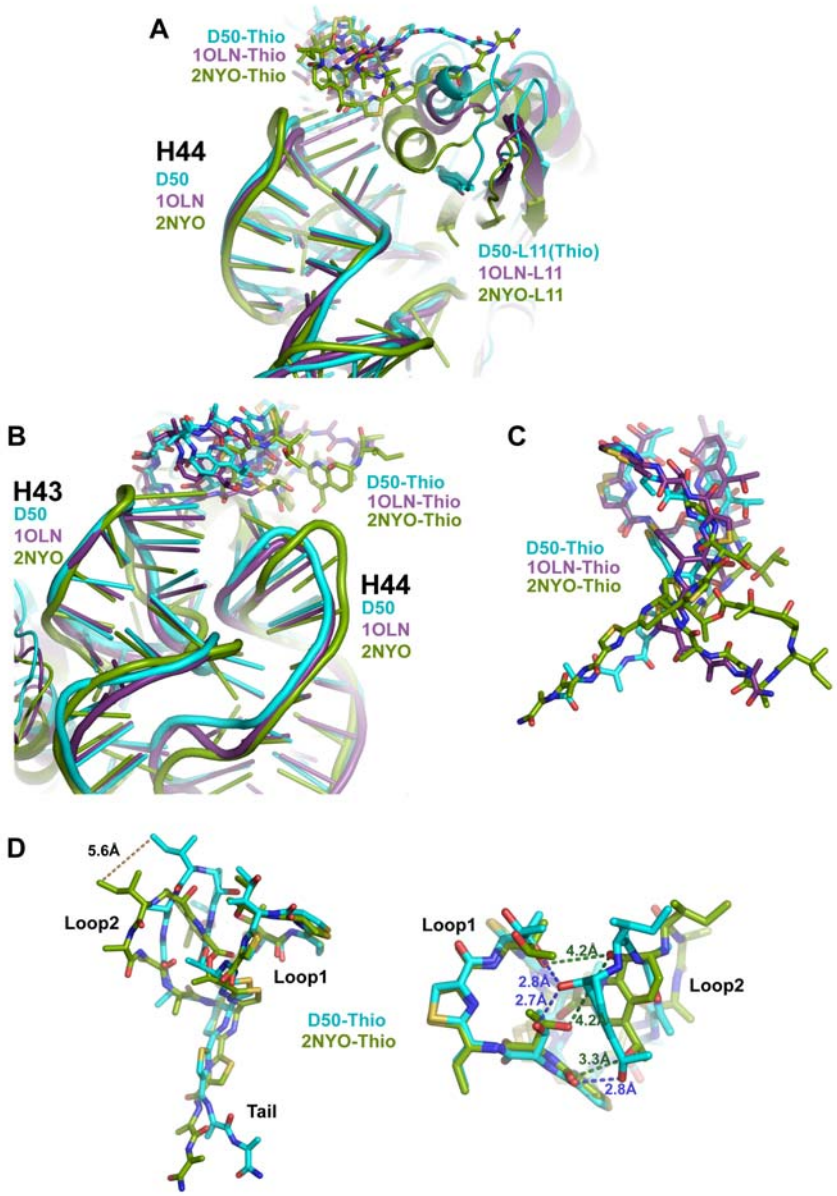

Supplemental Figure 1. Comparison of different Thio-rRNA models

(A) and (B) show two different views of the superposition of thiostrepton bound to the stalk base (SB) from NMR models PDB1OLN (purple) (Lentzen et al., 2003) and PDB2NYO (olive) (Jonker et al, 2007) with D50S-Thio structure (cyan). Alignments were made on the basis of H43 and H44 of the 23S rRNA.

(C) Comparison of the relative orientation and conformations of thiostrepton molecule from D50S-Thio (cyan), and NMR studies, coloured as in (A).

(D) In the study from Jonker et al, 2007 (PDB2NYO; olive), loop2 has shifted by up to 5.6 Å relative to loop1, when compared with the small molecule structure (data not shown) or D50S-Thio structure (cyan). This shift in loop2 leads to a loss in at least two, possibly three intramolecular hydrogen bonds that exist in the small molecule and D50S-Thio structures (cyan), as seen by the increase in distance from 2.7-2.8 Å (green) in the latter structures to 3.3-4.2 Å (blue) in the former structure.

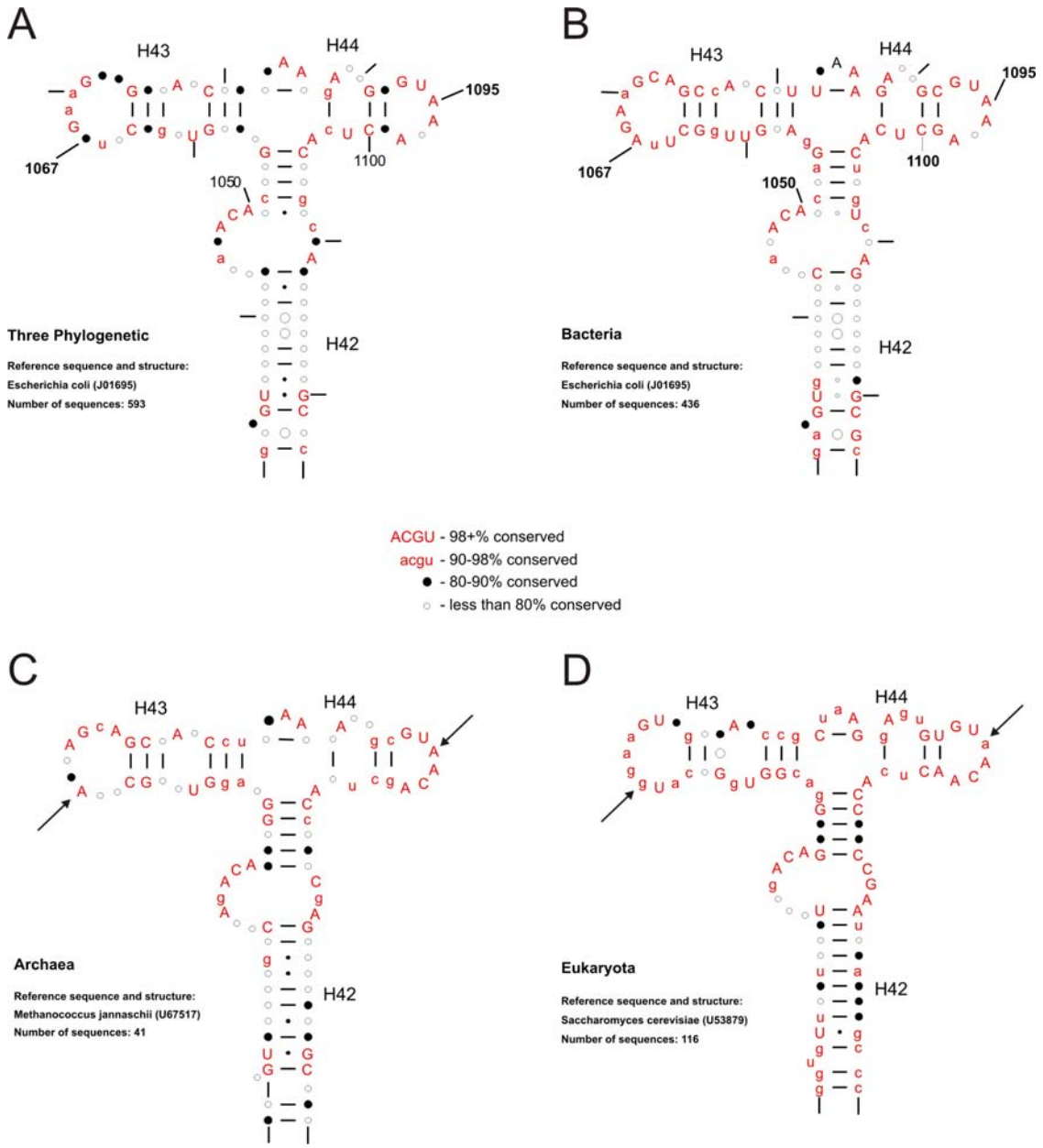

Supplemental Figure 2. Conservation of H43 and H44 in the 23S rRNA in prokaryotes and eukaryotes

Secondary structure of H42-H44 of the *E. coli* 23S rRNA, with the conservation of this region based on (A) all three phylogenic kingdoms (bacteria, archaea and eukaryotes), (B) 436 bacterial sequences, (C) 41 archaeal sequences and (D) 116 eukaryotic sequences. Note the universal conservation of A1067 and A1095 in bacteria as well as the equivalent positions in archaea (arrowed), but not in eukaryotes (arrowed). Upper and lower case letters indicate 98-100% and 90-98% conservation, respectively, whereas closed and open circles indicate conservation of 80-90% and less than 80%, respectively. The secondary structures and information were taken from http://www.rna.ccbb.utexas.edu/ (Cannone et al., 2002).

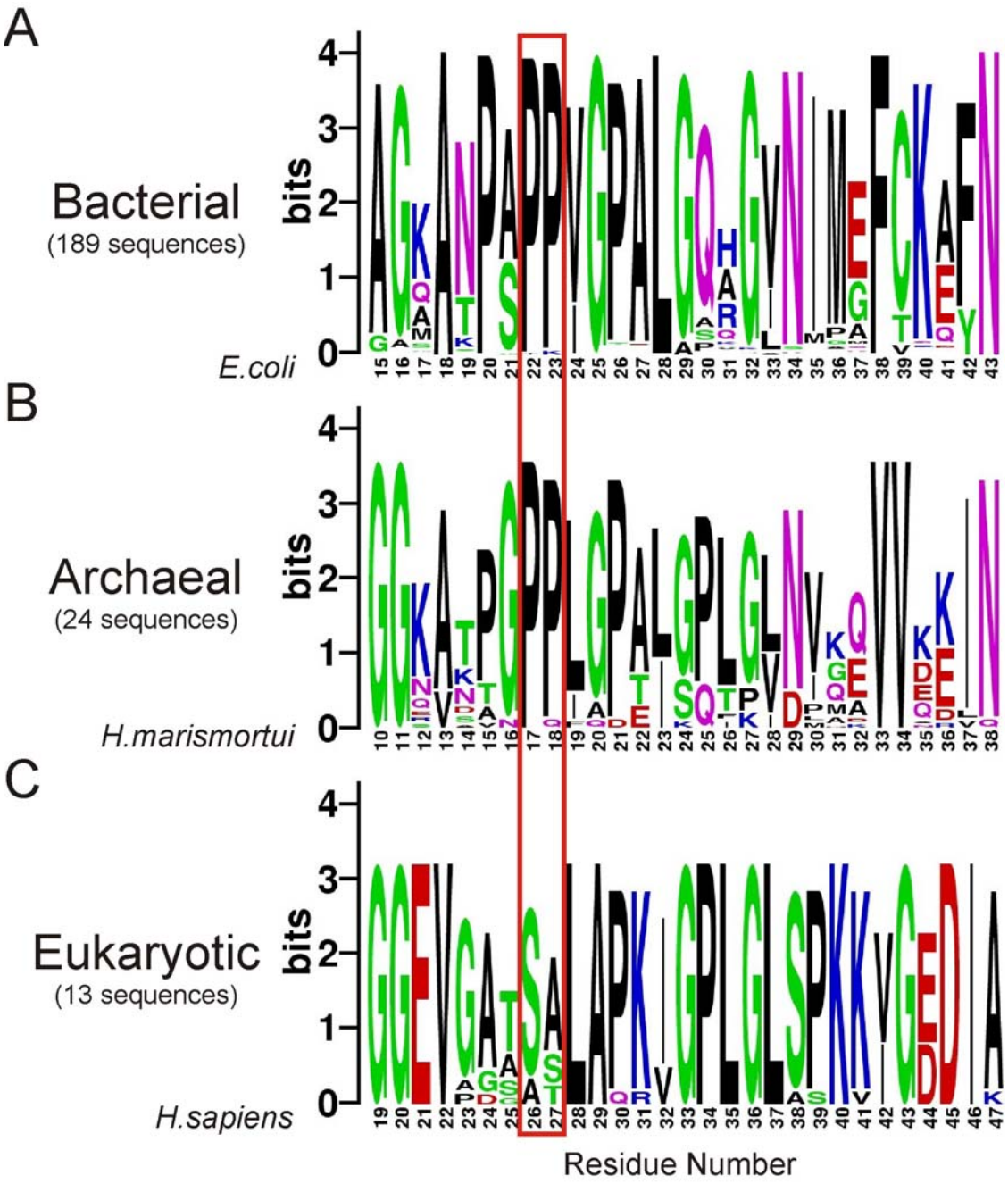

Supplemental Figure 3. Conservation of L11-NTD in bacteria, archaea and eukaryotes

Logo alignment of the N-terminal domain of r-protein L11 (L11-NTD) for (A) 189 bacterial, (B) 24 archaeal and (C) 13 eukaryotic sequences. The residues equivalent to *E. coli* proline 22 and 23 are indicated with a red box, highlighting the conservation of these prolines at the equivalent positions in archaea (*Haloarcula marismortui* numbering given) but not in eukaryotes (*Homo sapiens* numbering given). The logo alignment was made using the webserver http://weblogo.berkeley.edu/ (Crooks et al., 2004).

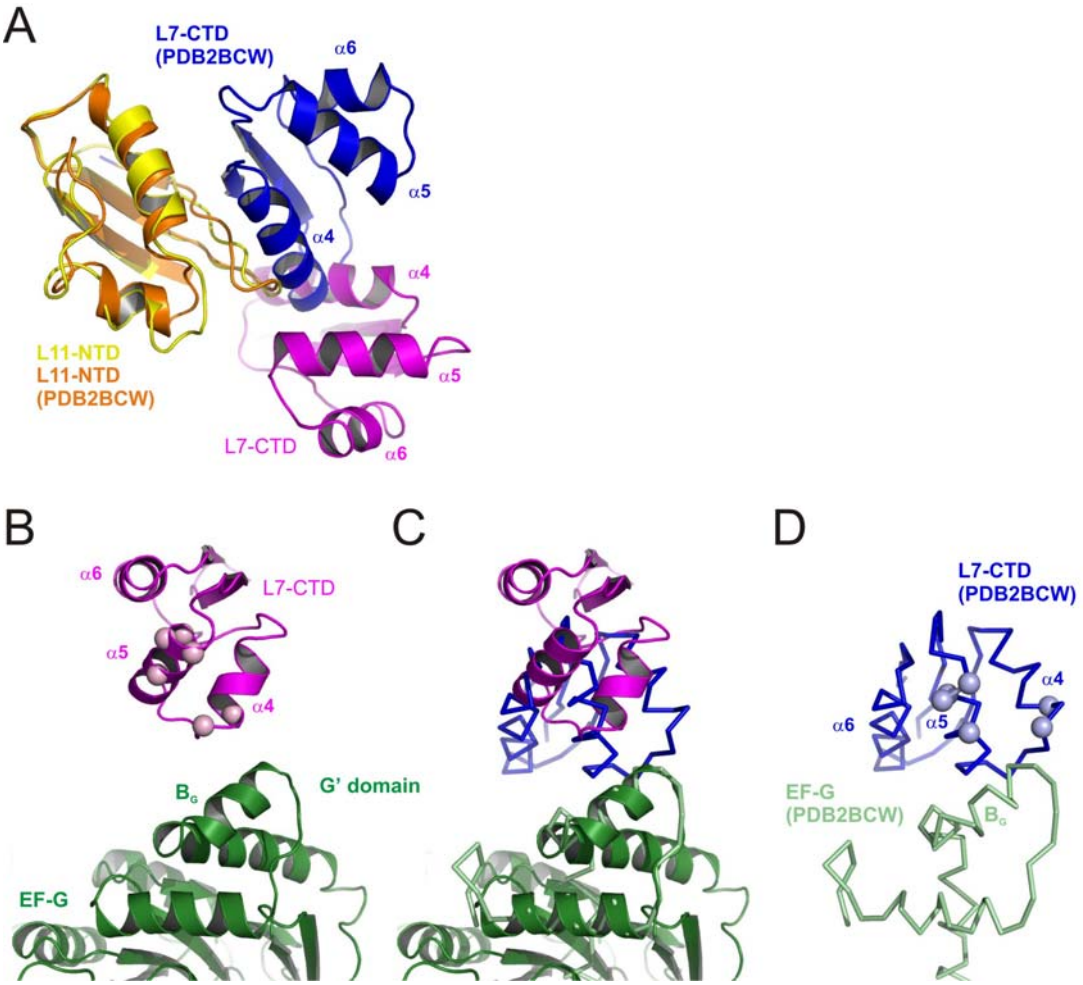

Supplemental Figure 4. Comparison of L7-CTD positions from crystal structure with cryo-EM

(A) Comparison of positions of L7-CTD (purple) from D50S-Micro crystal structure with L7-CTD (blue) taken from cryo-EM structure of EF-G•70S•fusidic acid complex (Datta et al., 2005); PDB2BCW), superimposed by aligning L11-NTD from D50S-Micro (yellow) and cryo-EM (orange; PDB2BCW) structures. Alpha-helices 4-6 are as indicated.

(B)-(D) Comparison of positions of L7-CTD with respect to the G' domain of EF-G.

(B) Relative positions of EF-G (green) and L7-CTD (magenta) based on model of D50S-Micro and cryo-EM EF-G•GDPNP•70S structure (Connell et al., 2007); PDB2OM7), with residues of L7-CTD implicated in EF-G interaction (Helgstrand et al., 2007) shown as pink spheres.

(C) Superimposition of (B) and (D)

(D) Relative positions of EF-G (pale green) and L7-CTD (blue) as determined by cryo-EM structure of EF-G•70S•fusidic acid complex (Datta et al., 2005); PDB2BCW), with residues of L7-CTD implicated in EF-G interaction (Helgstrand et al., 2007) shown as pale blue spheres.

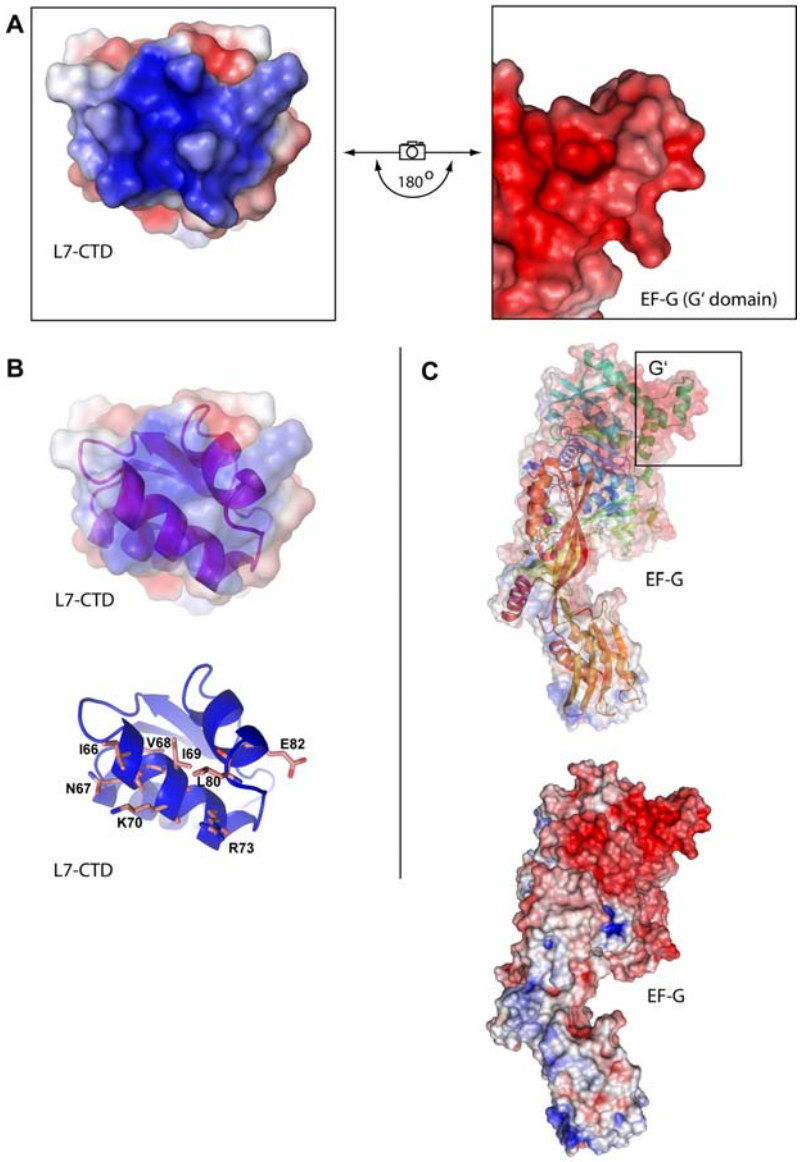

Supplemental Figure 5. Electrostatic potential of interaction surface between L7 and EF-G

(A) An "open-book" surface representation of L7-CTD (left) and G' domain of EF-G (right) showing the complementary positive (blue) and negative (red) electrostatic potential of the two interacting surfaces.

(B) Representation of L7-CTD as in (A), but with transparent surface to show the orientation of α-helices (upper panel) and position of residues (pink sticks) that have been implicated in EF-G interaction (Helgstrand et al., 2007) (lower panel).

(C) Representation of complete structure of EF-G with boxed region indicating G' domain shown in (A) and a transparent surface to show the ribbon representation (upper panel) and non-transparent surface to show electrostatic potential of entire EF-G molecule (lower panel).

Supplemental References

Cannone, J. J., Subramanian, S., Schnare, M. N., Collett, J. R., D'Souza, L. M., Du, Y., Feng, B., Lin, N., Madabusi, L. V., Muller, K. M., *et al.* (2002). The comparative RNA web (CRW) site: an online database of comparative sequence and structure information for ribosomal, intron, and other RNAs. BioMed Central Bioinformatics *3*, 2.

Connell, S. R., Takemoto, C., Wilson, D. N., Wang, H., Murayama, K., Terada, T., Shirouzu, M., Rost, M., Schuler, M., Giesebrecht, J., *et al.* (2007). Structural basis for interaction of the ribosome with the switch regions of GTP-bound elongation factors. Mol. Cell *25*, 751-764.

Crooks, G. E., Hon, G., Chandonia, J. M., and Brenner, S. E. (2004). WebLogo: a sequence logo generator. Genome Res. *14*, 1188-1190.

Datta, P. P., Sharma, M. R., Qi, L., Frank, J., and Agrawal, R. K. (2005). Interaction of the G' domain of elongation factor G and the C-terminal domain of ribosomal protein L7/L12 during translocation as revealed by cryo-EM. Mol. Cell *20*, 723-731.

Helgstrand, M., Mandava, C. S., Mulder, F. A., Liljas, A., Sanyal, S., and Akke, M. (2007). The ribosomal stalk binds to translation factors IF2, EF-Tu, EF-G and RF3 via a conserved region of the L12 C-terminal domain. J. Mol. Biol. *365*, 468-479.

Jonker, H. R., Ilin, S., Grimm, S. K., Wöhnert, J., Schwalbe, H. (2007) L11 domain rearrangement upon binding to RNA and thiostrepton studied by NMR spectroscopy. Nucleic Acids Res. *35*, 441-454.

Lentzen, G., Klinck, R., Matassova, N., Aboul-ela, F., and Murchie, A. (2003). Structural basis for contrasting activities of ribosome binding thiazole antibiotics. Chem. Biol. *10*, 769-778.